

Significant contribution of insolation to Eemian melting of the Greenland ice sheet

Willem Jan van de Berg^{1*}, Michiel van den Broeke¹, Janneke Ettema^{1,2}, Erik van Meijgaard³ and Frank Kaspar^{4,5}

During the Eemian interglacial period, 130,000 to 114,000 years ago, the volume of the Greenland ice sheet was about 30–60% smaller than the present-day volume^{1,2}. Summer temperatures in the Arctic region were about 2–4 K higher than today^{3–5}, leading to the suggestion that Eemian conditions could be considered an analogue for future warming⁶, particularly for the future stability of the Greenland ice sheet. However, Northern Hemisphere insolation was much higher during the Eemian than today, which could affect the reliability of this analogy. Here we use a high-resolution regional climate model with a realistic ice-sheet surface representation to assess the surface mass balance of the Greenland ice sheet during the Eemian. Our simulations show that Eemian climate led to an 83% lower surface mass balance, compared with the preindustrial simulation. Our sensitivity experiments show that only about 55% of this change in surface mass balance can be attributed to higher ambient temperatures, with the remaining 45% caused by higher insolation and associated nonlinear feedbacks. We show that temperature–melt relations are dependent on changes in insolation. Hence, we suggest that projections of future Greenland ice loss on the basis of Eemian temperature–melt relations may overestimate the future vulnerability of the ice sheet.

The mass balance of an ice sheet is equal to the sum of surface processes, that is, the surface mass balance (SMB = precipitation – sublimation – runoff), and solid ice discharge at the ice-sheet margins (Supplementary Fig. S1). The SMB of the Greenland ice sheet (GrIS) for the period 1961–1990 is estimated to be $479 \pm 53 \text{ Gt yr}^{-1}$, consisting of $701 \pm 42 \text{ Gt yr}^{-1}$ accumulation (precipitation minus sublimation) and $222 \pm 33 \text{ Gt yr}^{-1}$ runoff⁷ (Table 1). Assuming a zero ice-sheet mass balance for this period⁸ implies that solid ice discharge was close to 480 Gt yr^{-1} , comparable with independent estimates using satellite radar interferometry⁹. Precipitation and runoff dominate interannual variability in GrIS mass balance, with year-to-year SMB variations as large as $300\text{--}400 \text{ Gt yr}^{-1}$ (ref. 7). About 50% of the surface meltwater refreezes in the snowpack, making runoff the primary ablation component to consider in studies of GrIS SMB.

After 1990, GrIS runoff and solid ice discharge both increased, following atmospheric warming over Greenland^{10,11}, initiating a period of increasing mass loss that still continues today^{8,12,13}. The simultaneous post-1990 increase in runoff and solid ice discharge supports the observed coupling between runoff and basal sliding¹⁴ and warmer fjord waters thinning floating glacier tongues from below^{15–18}. For now, solid ice discharge remains the largest

component of annual GrIS mass loss. However, recent trends in runoff exceed those in solid ice discharge⁸, and in a future warmer climate, when the GrIS is expected to further retreat on land, runoff is likely to become the most important driver of GrIS mass loss.

An often-used analogue for the sensitivity of the GrIS to anthropogenic warming is its melt behaviour during the previous interglacial (Eemian, 130–114 kyr BP). Eemian near-surface summer temperatures were higher than today, by about 2 K in Europe and 2–4 K in the Arctic^{4,5}, comparable to the temperature rise in 2100 following Intergovernmental Panel on Climate Change projections for a business-as-usual scenario⁶. During the Eemian, global sea level peaked at levels that were 4–7 m above present^{19,20}. The contribution of the GrIS to this peak in Eemian sea level is estimated to range between 2.2 and 4.5 m, representing a loss of 30–60% of its present-day volume^{1,21,22}.

Here we investigate the validity of the Eemian melt analogy and the applicability of simple temperature–melt relations by calculating the GrIS SMB during the Eemian using the regional atmospheric climate model RACMO2/GR. This model explicitly and realistically quantifies all individual SMB components and subsurface processes at high horizontal resolution (18 km; ref. 7; Supplementary Figs S1, S2). Preindustrial and Eemian ambient atmospheric states from the general circulation model ECHO-G (ref. 23) were used as boundary conditions for 30-year-long RACMO2/GR simulations, of which the last 25 were analysed. For both ECHO-G and RACMO2/GR, the Eemian simulations were forced using the orbital parameters and greenhouse gas concentrations of 125 kyr BP (Supplementary Table S1). The present-day ice-sheet geometry²⁴ was maintained to rule out topographic effects. More information on the models and simulations is provided in the Methods section.

Eemian summertime top-of-atmosphere insolation in the Northern Hemisphere was up to 60 W m^{-2} higher than today (Fig. 1a). The ECHO-G simulations show that this results in summer ambient (500 hPa) temperatures over Greenland that were 3–4 K higher than in the preindustrial era (Fig. 1b). However, annual average ambient temperatures over the GrIS were only marginally different from the preindustrial, because of about 1 K colder winter and spring seasons. As a result, the Eemian climate has enhanced ambient-temperature seasonality over the ice sheet. Differences in 500 hPa geopotential height, with maxima over the Arctic basin and Newfoundland, show that the circumpolar circulation was weaker and less zonal during the Eemian summer (Fig. 1b).

Compared with the preindustrial, the impact of Eemian summer climate on GrIS SMB is very pronounced. Runoff dominates the response, visible as a substantial widening of the ablation zone

¹Utrecht University, Institute for Marine and Atmospheric Research (IMAU), PO Box 80005, 3508TA Utrecht, The Netherlands, ²University of Twente, Faculty of Geo-Information Science and Earth Observation (ITC), PO Box 217, 7500 AE Enschede, The Netherlands, ³Royal Netherlands Meteorological Institute, PO Box 201, 3730 AE De Bilt, The Netherlands, ⁴Max Planck Institute for Meteorology, Bundesstraße 53, 20146 Hamburg, Germany, ⁵Deutscher Wetterdienst, Frankfurter Straße 135, 63067 Offenbach, Germany. *e-mail: w.j.vandenberg@uu.nl

Table 1 | GrIS integrated SMB components (Gt yr^{-1}).

| Experiment | Present day | Preindustrial | Eemian | <i>Eem_Temp</i> | <i>Eem_Ins</i> |
|------------|--------------|---------------|--------------|-----------------|----------------|
| Insolation | Present day | Preindustrial | Eemian | Preindustrial | Eemian |
| Climate | 1961–1990 | Preindustrial | Eemian | Eemian | Preindustrial |
| Host model | ERA-40 | ECHO-G | ECHO-G | ECHO-G | ECHO-G |
| P – SU | 701 ± 42 | 594 ± 38 | 553 ± 37 | 558 ± 37 | 591 ± 38 |
| Runoff | 222 ± 33 | 148 ± 22 | 477 ± 67 | 311 ± 47 | 261 ± 39 |
| SMB | 479 ± 53 | 444 ± 44 | 74 ± 76 | 246 ± 60 | 329 ± 55 |

The uncertainty in accumulation (precipitation minus sublimation, P – SU) has been determined by comparing results from a present-day simulation with SMB observations following the method outlined in ref. 9. The uncertainty in runoff is estimated at 15%, on the basis of the standard deviation of recent model estimates (ref. 7, Supplementary Table S1, using updated values for MAR, X. Fettweis, personal communication).

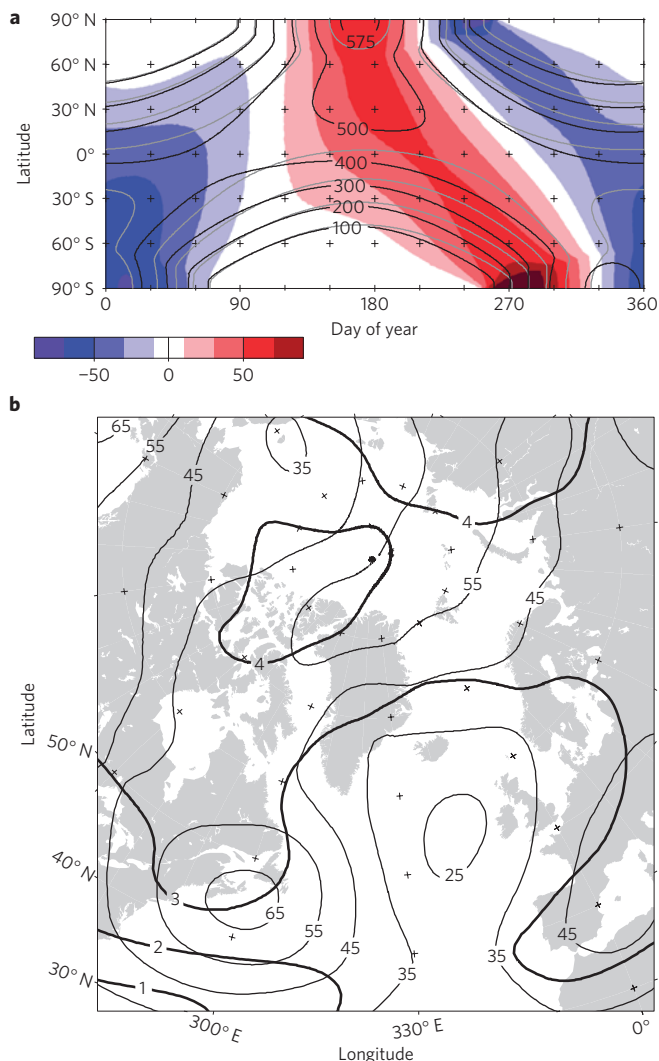


Figure 1 | Drivers of Eemian climate anomalies in Greenland. **a**, Annual cycle (on the basis of daily averages) of zonal average top-of-atmosphere insolation (W m^{-2}). Eemian insolation (black isolines, 100 W m^{-2} intervals), preindustrial insolation (grey isolines) and difference (colours). **b**, Summer (JJA) differences in 500 hPa temperature (K, thick lines) and 500 hPa geopotential height (m, thin lines) between the Eemian and preindustrial in ECHO-G.

(Fig. 2a,b). The SMB decreases by typically $500\text{--}1,000 \text{ kg m}^{-2} \text{ yr}^{-1}$ along the ice-sheet margins in the west, north and northeast (Fig. 2c). The equilibrium line moves upward by typically 500 m and inland by typically 100 km. As a result, the equilibrium line in

southwest Greenland is situated only 100 km from the ice divide. In contrast, snowfall rates in coastal southeast Greenland remain high enough to prevent the formation of a wide ablation zone.

Integrated over the GrIS, runoff more than triples compared with the preindustrial, forcing an impressive 83% decrease in SMB (Table 1). Interestingly, Eemian precipitation is lower compared with the preindustrial by 6%, challenging the often-made assumption that snowfall over the large ice sheets increases in a warmer climate. Weakened zonal circulation during the Eemian (Fig. 1b), producing less orographic precipitation, is the likely cause. Assuming, conservatively, an unchanged solid ice discharge of 479 Gt yr^{-1} , the Eemian GrIS mass loss would be close to 400 Gt yr^{-1} , equivalent to 1.1 m of global sea-level rise per millennium. This assumes unchanged topography: lowering the ice sheet would further accelerate melt. These numbers prove that a multiple-metre contribution of the GrIS to global sea-level rise during the Eemian is entirely plausible.

Eemian climate anomalies impact GrIS melt in two different ways: directly through stronger summertime insolation (Fig. 1a) and indirectly through higher ambient (free-atmosphere) temperatures (Fig. 1b). To isolate these effects, two further 30-year experiments, *Eem_Ins* and *Eem_Temp*, were carried out. In the *Eem_Ins* experiment, the insolation effect is quantified by prescribing Eemian insolation conditions at the top of the atmosphere, but retaining preindustrial climate lateral boundary forcings (Table 1, Fig. 2d). The *Eem_Temp* experiment quantifies the ambient-temperature effect, by retaining preindustrial insolation levels but applying the warmer Eemian climate forcing (Fig. 2e). Table 1 shows that the increase in runoff due to the insolation effect alone (*Eem_Ins*, $+113 \text{ Gt yr}^{-1}$) is very significant compared with the increase in runoff due to the ambient-temperature effect (*Eem_Temp*, $+163 \text{ Gt yr}^{-1}$). The reason for the pronounced effect of insolation is the snowmelt–albedo (α) feedback, expressing the fact that melting snow ($\alpha \approx 0.7$) absorbs approximately twice as much solar radiation as dry snow ($\alpha \approx 0.85$).

In the full Eemian experiment, the runoff anomaly increases by another 53 Gt yr^{-1} compared with the sum of changes in *Eem_Temp* and *Eem_Ins* (Table 1). This difference is caused by nonlinear feedbacks, notably the snowmelt–albedo feedback. In the full Eemian experiment, the melting anomaly extends further inland than in either the *Eem_Ins* or *Eem_Temp* simulations, which leads to activation of the snowmelt–albedo feedback over larger parts of the interior ice sheet. This effect is partly compensated by the reduced melt increase in the lower ablation zone due to double counting of the snowmelt–albedo feedback (Fig. 2f and Supplementary Fig. S3).

Our results suggest that Eemian-based temperature–melt relations would seriously overestimate melting in a future warmer climate, in which insolation at the top of the atmosphere remains approximately constant. To demonstrate this, we compare the runoff predicted by two commonly used temperature–melt relations with the runoff calculated by the (physical) regional climate

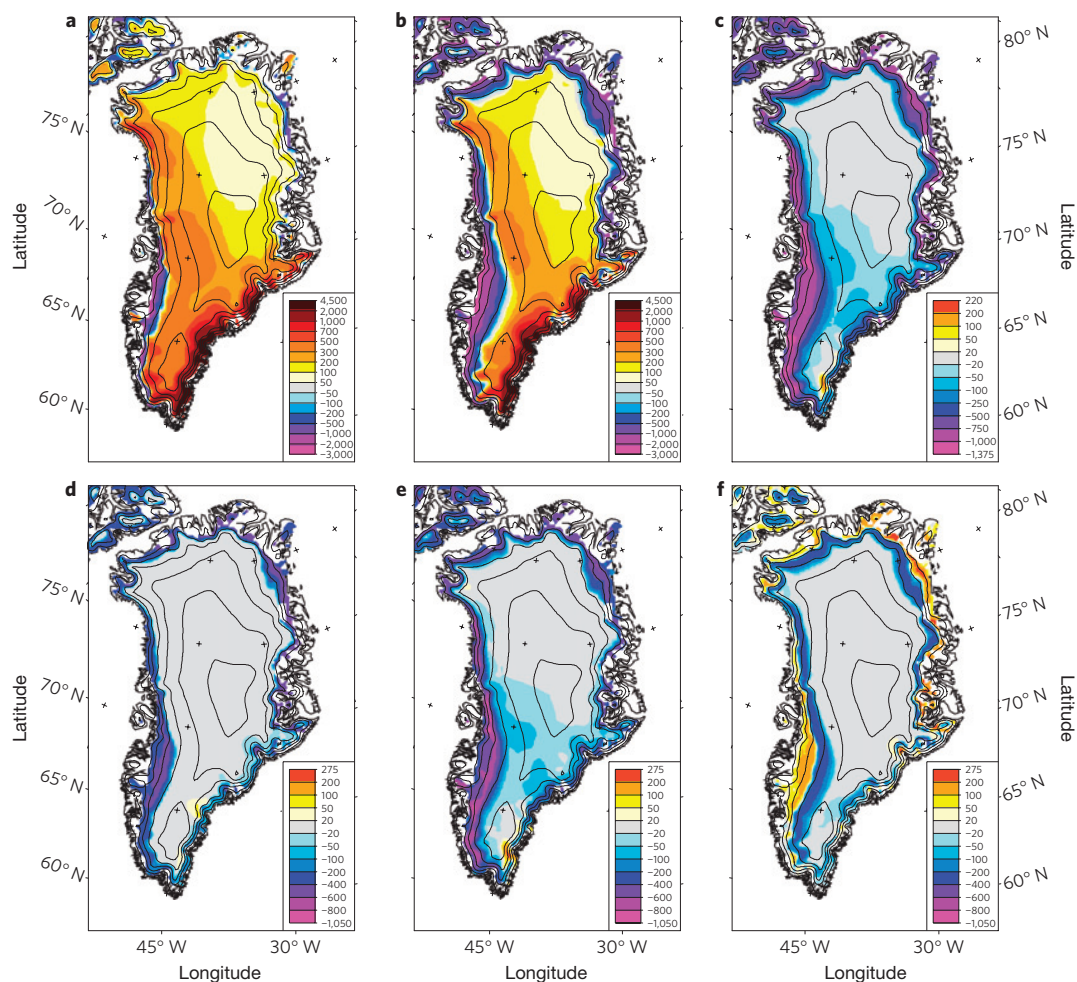


Figure 2 | Impact of Eemian climate anomalies on Greenland surface mass balance. a, b, GrIS SMB ($\text{kg m}^{-2} \text{yr}^{-1}$). **a**, Preindustrial. **b**, Eemian. **c–f**, Changes compared with preindustrial ($\text{kg m}^{-2} \text{yr}^{-1}$). **c**, Eemian. Note the absence of an accumulation increase in the ice-sheet interior. **d**, *Eem_Ins*. **e**, *Eem_Temp*. **f**, Nonlinear SMB response (preindustrial + Eemian - *Eem_Temp* - *Eem_Ins*). Ice-sheet elevation contours are given at 500 m intervals.

model. Temperature–melt relations are based on the fact that both 2 m temperature ($T_{2\text{m}}$) and surface melt rate are governed by the surface energy balance²⁵. Normally, temperature–melt relations are forced by simple, spatially uniform perturbations of $T_{2\text{m}}$ and prescribed snow/ice distributions, but here we force them with the more realistic $T_{2\text{m}}$ and snow/ice distributions from the regional climate model. Consequently, their performance is highly optimized.

The first temperature–melt relation directly couples average summer (June–July–August, JJA) $T_{2\text{m}}$ to runoff. Applying this method to our model results confirms that GrIS runoff anomalies, relative to preindustrial values, are correlated with JJA $T_{2\text{m}}$ anomalies (Fig. 3a). However, this relation is not unique: the two experiments with present-day insolation (preindustrial and *Eem_Temp*) show significantly lower summer runoff rates than the two simulations with Eemian insolation conditions (*Eem_Ins* and full Eemian). Note that JJA $T_{2\text{m}}$ is about 1 K higher in the *Eem_Ins* than in the preindustrial run. This temperature increase reflects the near-surface atmospheric response to the increased insolation, mainly in non-melting areas. In the regional climate model, these higher temperatures do not constitute a significant further forcing for melt (Supplementary Fig. S4a): nearly all the extra melt energy in *Eem_Ins* is provided by enhanced absorption of solar radiation. This result confirms that using an Eemian JJA temperature–runoff relation would significantly overestimate GrIS runoff sensitivity to near-future temperature changes under current insolation conditions.

The second temperature–melt relation couples the sum of positive degree-days to melt. We applied a full positive degree-day (PDD) calculation to daily model fields of $T_{2\text{m}}$ and melt, including the derivation of optimized PDD factors for snow and ice to match the melt in the regional climate model (see Methods section). These PDD factors, tuned for preindustrial conditions, were used to estimate GrIS melt for the *Eem_Temp*, *Eem_Ins* and full Eemian experiments (Fig. 3b). Given the different PDD factors for snow and ice, an assumption must be made about the snow/ice distribution. Here we used the snow/ice distributions from the regional climate model: the preindustrial snow/ice distribution serves to generate a low melt estimate (blue symbols in Fig. 3b) and the snow/ice distribution from the full Eemian experiment represents the most realistic alternative (red symbols in Fig. 3b). The melt amount from the regional climate model is represented by the black symbols. Despite correctly predicting *Eem_Temp* melt rate, the PDD method significantly underestimates melt for the experiments with Eemian insolation conditions, *Eem_Ins* and the full Eemian experiment. Conversely, overestimations of similar magnitude were found for the preindustrial and *Eem_Temp* experiments using PDD factors tuned for Eemian conditions. Moreover, the PDD method fails to correctly capture the north–south melt gradient, which is driven by insolation gradients (Supplementary Fig. S5).

Supplementary Fig. S6 illustrates the fundamental problem of temperature–melt relations, that is the weak relation between melt rate and $T_{2\text{m}}$, for both snow and ice surfaces. For example, if $T_{2\text{m}}$

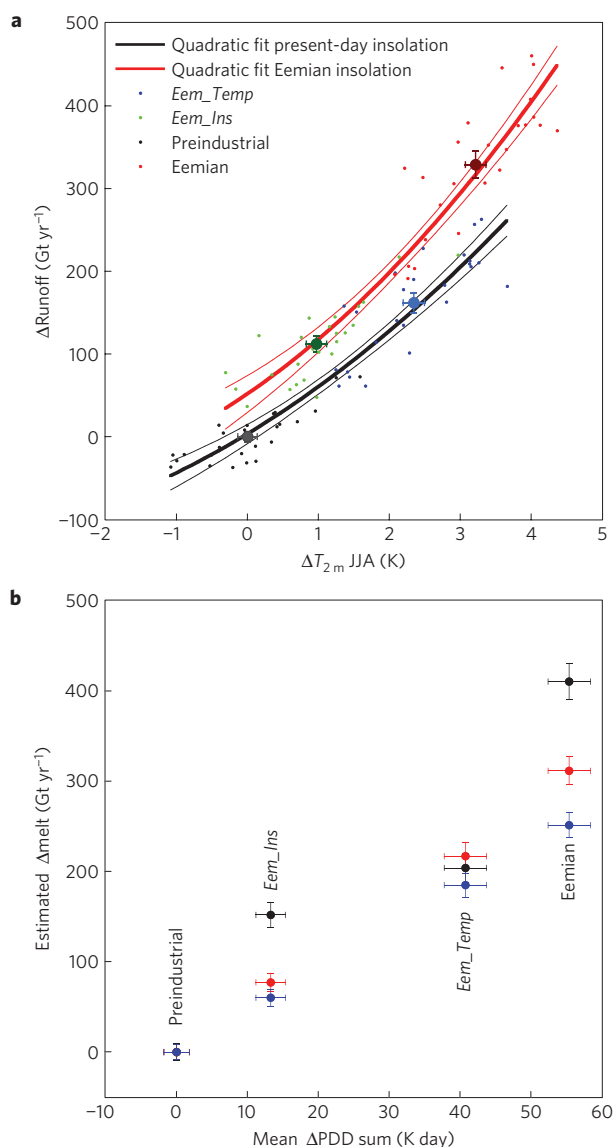


Figure 3 | Evaluation of temperature-melt methods. **a**, Anomalies of GrIS runoff as a function of anomaly in 2 m temperature (T_{2m}), relative to the preindustrial values. The small dots represent individual years; the larger symbols represent period averages. Error bars signify the standard error due to interannual variability. **b**, GrIS melt anomalies using the PDD method tuned for preindustrial climate. Shown are means with standard error, using the preindustrial snow/ice distribution (blue symbols) and the snow/ice distribution from the experiment (red symbols). Black symbols represent melt from the full model.

exceeds 0°C , melt does not necessarily occur. Temperature-melt relations assume that the shared dependence of T_{2m} and melt rate on the surface energy balance enables the use of a fixed relation between the two, but ignore that this relation depends, among other factors, on insolation, hence orbital parameters and latitude (Supplementary Fig. S5). For the two temperature-melt relations investigated here, for the Eemian the systematic bias amounts to at least 25% of the total melt/runoff change (Fig. 3). Given the elaborate optimization process that is based on information that normally is not available, this must be regarded as a lower limit.

In summary, our results support previous findings that rapid melting of the GrIS did occur during the Eemian. However, enhanced summer insolation caused an important part of this strong sensitivity. We show that fixed temperature-melt relations,

like the PDD method, are unable to predict melt correctly once insolation has changed. This is why the Eemian melt-temperature relation provides a poor analogue of a future warmer climate, in which insolation at the top of the atmosphere remains approximately constant compared with today.

Methods

Regional Atmospheric Climate Model. In this study the Regional Atmospheric Climate Model version 2.1 (RACMO2) of the Royal Netherlands Meteorological Institute (KNMI) is used to simulate the climate and SMB of the GrIS. RACMO2 is in fact a combination of two numerical weather prediction models: the atmospheric dynamics originate from the High Resolution Limited Area Model (HIRLAM, version 5.0.6; ref. 26), whereas the description of the physical processes is adopted from the global model of the European Centre for Medium-Range Weather Forecasts (ECMWF, updated cycle 23r4; ref. 27). At the lateral boundaries, prognostic atmospheric fields from ECHO-G force the model every 6 h, whereas the interior of the domain is allowed to evolve freely. No observations are assimilated within the domain during the simulations with RACMO2. General adjustments to the original formulas of the dynamical and physical schemes in RACMO2 are described in detail in ref. 28. The adjustments to the original model formulation that have been made to better represent the conditions in the Arctic region (RACMO2/GR) are described in Supplementary Information.

Simulation set-up. RACMO2/GR was nested into the 3.75° ECHO-G model data. The lateral boundary condition fields from ECHO-G comprise temperature, humidity, wind and surface pressure; lower boundary conditions are sea surface temperature and sea-ice fraction. A description of the ECHO-G model is given in Supplementary Information. Sea-ice fraction and sea surface temperature were interpolated from ECHO-G output. Ideally, glaciated grid box surfaces are initialized either with a developed snow pack in the accumulation zone, or with bare ice in the ablation zone. As the equilibrium line is unknown before a simulation, such initial preconditioning is not allowed. Therefore, all glaciated grid boxes were initialized with 1 m of snow and firn on top of a thick ice layer. Although 1 m of snow over ice already captures most of the thermal characteristics of a fully developed snow pack, it can also easily melt away if the grid point belongs to the ablation zone. The snow/ice-pack temperature was initialized using the parameterization of ref. 29, including a correction for refreezing. However, the effect of deep ice temperature on the final SMB is very small. To avoid spin-up effects, only the last 25 years of the 30 year simulations were used.

In Supplementary Information further testing of the simulation set-up is discussed. Furthermore, the SMB estimate of preindustrial climate using ECHO-G boundaries is evaluated compared with the RACMO2/GR estimate of present-day SMB.

Uncertainty interval in quadratic fits. The 95% confidence intervals (thin lines) of the quadratic fits in Fig. 3a were calculated using

$$\hat{R}|_{T_i} = \alpha + \beta T_i + \gamma T_i^2 \pm t_{n-3}^* \sqrt{\frac{1}{n-3} \sum e_i^2 \left(\frac{1}{n} + \frac{(T_i - T_m)^2}{\sum (T_i - T_m)^2} + \frac{(T_i - T_m)^4}{\sum (T_i - T_m)^4} \right)}$$

in which $\hat{R}|_{T_i}$ is the confidence interval for temperature T_i ; α , β and γ are fit parameters; T_i and T_m are the individual and average T_{2m} values, respectively; e_i is the difference of an individual melt value from the fit; n is the number of data points ($n=50$); t^* is the Student t -statistic for $n-3$ degrees of freedom ($t^*=2.01$).

The PDD method. We applied a full PDD calculation to daily model fields of T_{2m} and melt (that is 4,610,700 daily values covering 25 years using the 360 day model calendar). First, we derived optimal preindustrial PDD factors for snow and ice by matching GrIS integrated melt with PDD sums. For many ice-sheet locations, melt occurs only during part of the day, so that using a threshold of 273.15 K for daily mean T_{2m} misses melt events and reduces the predictive strength of the PDD method³⁰. A threshold of 269.5 K for daily mean T_{2m} provided the best melt prediction for both interannual variability ($r=0.93$, root mean squared error, RMSE = 16 Gt yr^{-1}) and the spatial melt distribution (RMSE = 85 mm yr^{-1} , average error 39 mm yr^{-1}). These PDD factors were used to estimate GrIS melt for the Eem_Temp, Eem_Ins and full Eemian experiments (Fig. 3b). The assumptions made about the snow/ice distribution are described in the main text. Figure 3b shows that the PDD method successfully predicts GrIS melt in the Eem_Temp experiment, which uses present-day insolation. From this we could conclude that the PDD method is capable of predicting GrIS melt amounts for a wide range of 2 m temperature perturbations, provided that (1) PDD factors are optimized to match the current GrIS melt amounts, (2) insolation remains constant and (3) the snow/ice distribution is always known. However, this interpretation overlooks the fact that an important latitudinal insolation gradient exists over the GrIS: the use of constant PDD factors leads to significantly overestimated (underestimated) melt amounts in the northern (southern) parts of the ice sheet (Supplementary Fig. S5). This further stresses the importance of using a realistic spatial-temporal

distribution of insolation to calculate GrIS melt. Moreover, the PDD method only predicts melt, so further assumptions must be made about the refreezing of meltwater to obtain runoff.

Received 17 January 2011; accepted 1 August 2011; published online 4 September 2011

References

- Overpeck, J. T. *et al.* Paleoclimatic evidence for future ice-sheet instability and rapid sea-level rise. *Science* **311**, 1747–1750 (2006).
- Robinson, A., Calov, R. & Ganopolski, A. Greenland Ice Sheet model parameters constrained using simulations of the Eemian Interglacial. *Clim. Past Discuss.* **6**, 1551–1588 (2010).
- Jansen, E. *et al.* in *IPCC Climate Change 2007: The Physical Science Basis* (eds Solomon, S. D. *et al.*) (Cambridge Univ. Press, 2007).
- Kaspar, F. & Cubasch, U. in *The Climate of Past Interglacials* Vol. 7 (eds Sirocko, F., Litt, T., Claussen, M. & Sánchez-Goni, M. F.) Ch. 33, 499–515 (Developments in Quaternary Sciences, Elsevier, 2007).
- Otto-Bliesner, B. L. *et al.* Simulating Arctic climate warmth and icefield retreat in the last interglaciation. *Science* **311**, 1751–1753 (2006).
- Meehl, G. A. *et al.* in *IPCC Climate Change 2007: The Physical Science Basis* (eds Solomon, S. D. *et al.*) (Cambridge Univ. Press, 2007).
- Ettema, J. *et al.* Higher surface mass balance of the Greenland ice sheet revealed by high-resolution climate modeling. *Geophys. Res. Lett.* **36**, L12501 (2009).
- Van den Broeke, M. R. *et al.* Partitioning recent Greenland mass loss. *Science* **326**, 984–986 (2009).
- Rignot, E. *et al.* Mass balance of the Greenland ice sheet from 1958 to 2007. *Geophys. Res. Lett.* **35**, L20502 (2008).
- Box, J. E. & Cohen, A. E. Upper-air temperatures around Greenland: 1964–2005. *Geophys. Res. Lett.* **33**, L12706 (2006).
- Hanna, E. *et al.* Increased runoff from melt from the Greenland ice sheet: A response to global warming. *J. Clim.* **21**, 331–341 (2008).
- Fettweis, X. Reconstruction of the 1979–2006 Greenland ice sheet surface mass balance using the regional climate model MAR. *Cryosphere* **1**, 21–40 (2007).
- Velicogna, I. Increasing rates of ice mass loss from the Greenland and Antarctic ice sheets revealed by GRACE. *Geophys. Res. Lett.* **36**, L19503 (2009).
- Sundal, A. V. *et al.* Melt-induced speed-up of Greenland ice sheet offset by efficient subglacial drainage. *Nature* **469**, 521–524 (2011).
- Thomas, R. H. Force-perturbation analysis of recent thinning and acceleration of Jakobshavn Isbrae, Greenland. *J. Glaciol.* **50**, 57–66 (2004).
- Holland, D. M. *et al.* Acceleration of Jakobshavn Isbrae triggered by warm subsurface ocean waters. *Nature Geosci.* **1**, 659–664 (2008).
- Murray, T. *et al.* Ocean regulation hypothesis for glacier dynamics in southeast Greenland and implications for ice sheet mass changes. *J. Geophys. Res.* **115**, F03026 (2010).
- Rignot, E., Koppes, M. & Velicogna, I. Rapid submarine melting of the calving faces of West Greenland glaciers. *Nature Geosci.* **3**, 187–191 (2010).
- Lhomme, N. *et al.* Tracer transport in the Greenland Ice Sheet: Constraints on ice cores and glacial history. *Quat. Sci. Rev.* **24**, 173–194 (2005).
- Kopp, R. E. *et al.* Probabilistic assessment of sea level during the last interglacial stage. *Nature* **462**, 863–867 (2009).
- Cuffey, K. M. & Marshall, S. J. Substantial contribution to sea-level rise during the last interglacial from the Greenland ice sheet. *Nature* **404**, 591–594 (2000).
- Tarasov, L. & Peltier, W. R. Greenland glacial history, borehole constraints, and Eemian extent. *J. Geophys. Res.* **108**, 2143 (2003).
- Kaspar, F., Kühl, N., Cubasch, U. & Litt, T. A model–data comparison of European temperatures in the Eemian interglacial. *Geophys. Res. Lett.* **32**, L11703 (2005).
- Bamber, J. L., Ekholm, S. & Krabill, W. B. A new, high-resolution digital elevation model of Greenland fully validated with airborne altimeter data. *J. Geophys. Res.* **106**, 6733–6745 (2001).
- Ohmura, A. Physical basis for the temperature-based melt-index method. *J. Appl. Meteorol.* **40**, 753–761 (2001).
- Undén, P. *et al.* *High Resolution Limited Area Model, HiRLAM-5 Scientific Documentation*. Tech. Rep. (Swed. Meteorol. and Hydrol., 2002).
- IFS Documentation CY23R4: Part IV Physical Processes (see <http://www.ecmwf.int/research/ifsdocs>) (2004).
- Van Meijgaard, E. *et al.* *The KNMI Regional Atmospheric Climate Model RACMO version 2.1*, Tech. Rep. (2008).
- Reeh, N. Parameterization of melt rate and surface temperature on the Greenland ice sheet. *Polarforschung* **59**, 113–128 (1991).
- Van den Broeke, M. R., Bus, C., Ettema, J. & Smeets, P. Temperature thresholds for degree-day modelling of Greenland ice sheet melt rates. *Geophys. Res. Lett.* **37**, L18501 (2010).

Acknowledgements

This work is funded by Utrecht University and the Polar Program of the Netherlands Organization for Scientific Research, section Earth and Life Sciences (NWO/ALW).

Author contributions

All authors discussed the results and commented on the manuscript. W.J.v.d.B. and M.v.d.B. wrote the paper and integrated the results, W.J.v.d.B. carried out RACMO2/GR calculations and the temperature–melt analysis, M.v.d.B., W.J.v.d.B., J.E. and E.v.M. contributed to the development of RACMO2/GR and F.K. provided ECHO-G boundary fields.

Additional information

The authors declare no competing financial interests. Supplementary information accompanies this paper on www.nature.com/naturegeoscience. Reprints and permissions information is available online at <http://www.nature.com/reprints>. Correspondence and requests for materials should be addressed to W.J.v.d.B.